AJNR

Comparison of HASTE versus EPI-Based DWI for Retinoblastoma and Correlation with Prognostic Histopathologic Parameters

Manish Sharma, Amit Gupta, Manisha Jana, Seema Kashyap, Sameer Bakhshi and Sanjay Sharma

AJNR Am J Neuroradiol published online 4 January 2024
http://www.ajnr.org/content/early/2024/01/04/ajnr.A8084

Published January 4, 2024 as 10.3174/ajnr.A8084

Comparison of HASTE versus EPI-Based DWI for Retinoblastoma and Correlation with Prognostic Histopathologic Parameters

Manish Sharma, Amit Gupta, Manisha Jana, Seema Kashyap, Sameer Bakhshi, and Sanjay Sharma

ABSTRACT

BACKGROUND AND PURPOSE: Non-EPI-based DWI has shown better performance in head and neck pathologies owing to lesser susceptibility artifacts compared with EPI-DWI. However, only sporadic studies have investigated the feasibility of non–EPI-based DWI in retinoblastoma (RB). We qualitatively and quantitively compared EPI-DWI and HASTE-DWI in RB and correlated the tumor ADC values obtained from these 2 techniques with histopathologic markers.

MATERIALS AND METHODS: Twenty-one treatment-naive patients with RB underwent 1.5T orbital MR imaging. EPI-DWI and HASTE-DWI were acquired at 3 b-values (0, 500, and 1000 s/mm^2). All patients subsequently underwent surgical enucleation. For qualitative image assessment, scoring of overall image quality, artifacts, tumor sharpness, and tumor conspicuity was done by using a 5-point Likert scale. Quantitative assessment included calculations of SNR, contrast-to-noise ratio (CNR), geometric distortion, and ADC. Qualitative scores were compared by using the Wilcoxon signed-rank test, and quantitative parameters were analyzed with a *t* test.

RESULTS: All 21 patients had unilateral RB; 15 were male and 6 were female with a median age of 36 months (range, 9–72 months). On histopathology, patients had either poorly differentiated ($n = 13/21$) or moderately differentiated ($n = 8/21$) RB. Other poor prognostic markers evaluated were optic nerve invasion ($n = 10/21$), choroidal invasion ($n = 12/21$), and anterior eye segment enhancement on MRI ($n = 6/21$). HASTE-DWI demonstrated higher image quality scores than EPI-DWI ($P < .01$), except for tumor conspicuity score, which was higher for EPI-DWI ($P < .001$). HASTE-DWI showed lower SNR, CNR, and geometric distortion than EPI-DWI ($P < .001$). The average acquisition times of EPI-DWI and HASTE-DWI were ~1 and 14 minutes, respectively. The mean tumor ADC value on EPI-DWI was $0.62 \pm 0.14 \times 10^{-3}$ mm^2/s and on HASTE-DWI was $0.83 \pm 0.17 \times 10^{-3}$ mm^2/s. A significant correlation between EPI-DWI and HASTE-DWI ADC values ($r = 0.8$; $P = .01$) was found. Lower ADC values were found in tumors with poor prognostic markers, but none reached a statistically significant difference.

CONCLUSIONS: HASTE-DWI shows improved overall image quality; however, it lacks in terms of tumor conspicuity, SNR, CNR, and longer acquisition time compared with EPI-DWI. ADC values derived from HASTE-DWI show no advantage over EPI-DWI in correlation with histopathologic prognostic markers.

ABBREVIATIONS: CNR = contrast-to-noise ratio; EPI-DWI = EPI-based DWI; RB = retinoblastoma

DWI is an fMRI technique based on Brownian motion of water molecules within the tissues. ADC value derived from DWI is an objective measure of free diffusion in the tissue.[1] There is abundant literature available on the utility of DWI for detection and characterization of various neoplasms, including malignant and benign orbital masses.[1-5] In retinoblastoma (RB), a fair correlation of tumor ADC values has been shown with poor prognostic markers, such as poorly differentiated tumor on histopathology, tumor bilaterality, optic nerve invasion, and choroidal invasion.[6-8] However, the studies report a wide range of ADC values (0.38×10^{-3} to 0.74×10^{-3} mm^2/s) associated with these markers with no consistent definite cutoff values.[6,7] Nonetheless, tumor ADC values could have implications for medical and surgical management of RB.

The most commonly used EPI-based DWI (EPI-DWI) sequences allow short scan times but have marked susceptibility

Received September 8, 2023; accepted after revision October 29.

From the Departments of Radiodiagnosis and Interventional Radiology (M.S., A.G., M.J., S.S.), and Pathology (S.K.), All India Institute of Medical Sciences, New Delhi, India; and Department of Medical Oncology (S.B.), Institute of Rotary Cancer Hospital, All India Institute of Medical Sciences, New Delhi, India.

M. Sharma and A. Gupta contributed equally to this work as co-first authors.

Please address correspondence to Prof. Sanjay Sharma, Room 53, Dr. R. P. Centre for Ophthalmic Sciences, Department of Radiodiagnosis, All India Institute of Medical Sciences, New Delhi, Ansari Nagar 110029, India; e-mail: drssharma11@gmail.com

Indicates article with online supplemental data.

http://dx.doi.org/10.3174/ajnr.A8084

artifacts, especially at bone–air interfaces. Substantial anatomic distortion on orbital EPI-DWI is well known.[9] The use of non–EPI-based DWI for head and neck pathologies is well documented, especially for diagnosis of recurrent postoperative cholesteatomas, where it has been shown to outperform the traditional EPI-DWI in terms of image quality as well as diagnostic sensitivity and specificity.[10,11] HASTE-DWI is one such non-EPI technique, which has been in use for many years and is currently considered the reference standard MR imaging sequence for detection of cholesteatomas.[12,13] Similarly in cases of RB, we hypothesize that HASTE-DWI could potentially facilitate better coregistration with conventional MR images with better visual tumor delineation and perhaps provide a more robust ADC value correlation as an imaging prognostic marker. However, the use of non–EPI-based DWI for detection and characterization of RB has been reported only in few preliminary studies with limited sample sizes.[14,15]

To the best of our knowledge, there is no study available in the literature comparing both EPI-DWI and HASTE-DWI in the same patients with RB cohort. Also, there are no data regarding the correlation of prognostic markers in RB with ADC values derived from HASTE-DWI. The purpose of our study was to qualitatively and quantitatively compare the images acquired from EPI-DWI and HASTE-DWI in eyes with RB and correlate the derived ADC values with histopathologic prognostic markers.

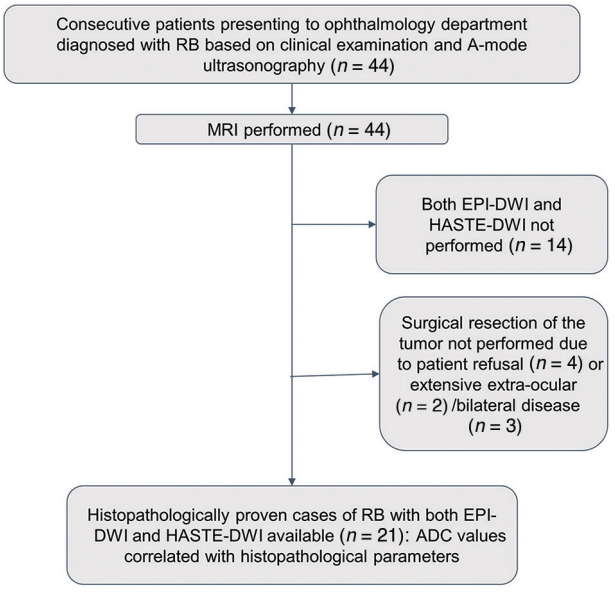

FIG 1. Flow chart showing patient inclusion and exclusion in the study.

MATERIALS AND METHODS

This prospective observational study was conducted after obtaining Institutional Ethics Committee approval. After taking informed parental consent, a total of 44 consecutive children with RB referred for MR imaging from our tertiary care ophthalmology center were recruited. The diagnosis of RB was based on clinical examination and A-mode ultrasonography. Patients who did not undergo surgical enucleation ($n = 9$) because of either extensive bilateral/extra-ocular disease or guardian's refusal were excluded. Also, the patients in whom both EPI-DWI and HASTE-DWI could not be performed ($n = 14$) were excluded from the study. Thus, a total of 21 treatment-naive patients with RB formed the final study group (Fig 1). There was no minimum tumor size criterion for inclusion into the study analysis.

Orbital MR imaging was performed under general anesthesia by using a 1.5T system (Avanto; Siemens) with a standard quadrature head coil (FOV 20 cm). Conventional sequences included thin-section spin-echo fat-suppressed T2-weighted orbital images in axial, coronal, and oblique sagittal planes, fat-suppressed T1-weighted orbital images in the axial plane followed by postcontrast orbital fat-suppressed T1-weighted images in all 3 planes, and postcontrast brain imaging after intravenous administration of gadopentetate dimeglumine (Magnevist). DWI ($n = 21$) of the orbits was acquired in the axial plane with b-values of 0, 500, and 1000 mm^2/s by using both EPI-DWI and HASTE-DWI (Online Supplemental Data). ADC maps were generated automatically for EPI-DWI and manually for HASTE-DWI.

Qualitative image assessment was performed by a radiologist (S.S., with 20 years' experience in orbital imaging) on the $b = 1000$ s/mm^2 images. The overall image quality, artifacts, tumor sharpness, and tumor conspicuity were scored by using a 5-point Likert scale as shown in Table 1. For quantitative image quality assessment, a single radiologist (A.G., with 8 years' experience in body imaging) placed ROIs on the tumor and temporalis muscle in the same axial section to measure the signal values on $b = 0$ s/mm^2 images on both EPI-DWI and HASTE-DWI and subsequently transferred the same ROIs to corresponding $b = 500$ and 1000 s/mm^2 images (Online Supplemental Data). SNR was defined as signal of tumor divided by the SD. Contrast-to-noise ratio (CNR) was defined as the absolute signal difference of tumor and muscle divided by the SD of muscle signal. For quantification of geometric distortion (measured by a single radiologist A.G., with 8 years' experience in body imaging), the maximum transverse and anteroposterior diameters of the eye globe on axial T2-weighted images were taken as the standard of reference. The distortion was assessed by measuring the deviations in the orbital diameters on both EPI-DWI and HASTE-DWI on the same axial section as T2-weighted image.

Table 1: Qualitative image assessment based on the 5-point Likert scale

Score	Overall Image Quality	Artifacts	Tumor Sharpness	Tumor Conspicuity
1	Nondiagnostic	Nondiagnostic	Nondiagnostic	Mass unidentifiable
2	Substantial deficiency in image quality	Marked impact on diagnosis	Not sharp	No differentiation between mass and vitreous
3	Moderate image quality	Moderate impact on diagnosis	Little sharp	Subtle mass lesion
4	Good image quality	Minimal impact on diagnosis	Moderately sharp	Well-seen mass lesion
5	Excellent image quality	No artifact	Good sharpness	Very well-seen mass lesion

Table 2: Patient characteristics ($n = 21$)

Characteristic	Value
Median age at enucleation	36 months (range, 9–72 months)
Sex	Male: 15 (71.4%) Female: 6 (29.6%)
Tumor laterality	Unilateral: 21 (100%) Bilateral: 0 Right eye: 13 (61.9%) Left eye: 8 (38.1%)
Median tumor size	15.3 mm (range, 10.2–36 mm)
Mean follow-up period	265.4 days (range, 155–410 days)

Quantitative analysis of the ADC map was performed by a single radiologist (M.S., with 10 years' experience in pediatric body imaging). Three circular ROIs of 0.12 cm^2 size were placed manually over the mass on the ADC map with simultaneous referencing of the T2-weighted and postcontrast images. Tumor ADC values were calculated as a mean of these 3 ROIs. The ROIs were drawn corresponding to the enhancing portion of the mass. Areas showing high signal on T2-weighted images with scarce or no contrast enhancement were considered as necrotic areas and were avoided during ROI placement. Similarly, dark foci suspicious of calcifications were not included in the ROI.

The postcontrast MR images were assessed for anterior eye segment enhancement by a single radiologist (M.S., with 20 years' experience in orbital imaging). Anterior eye segment enhancement was considered positive if there was an abnormal high signal on postcontrast MR imaging just anterior to the lens in the axial section showing maximum cross-section of the lens (ie, in the location of iris).

All patients underwent surgical enucleation, either upfront or preceded by neoadjuvant chemotherapy, within 20–30 days (mean duration of 27.1 days) after MR imaging. Various histopathologic parameters were evaluated. Tumor grade was classified as well (>50% rosettes), moderately (<50% rosettes), or poorly (no rosettes) differentiated. Optic nerve invasion was categorized as absent, prelaminar (optic nerve head), and postlaminar. Choroidal invasion was also noted. Invasion of iris, ciliary body, anterior chamber, and sclera was also assessed.

Qualitative scores were compared by using the Wilcoxon signed-rank test, and quantitative image quality parameters (SNR, CNR, and geometric distortion) were compared with a paired *t* test after testing for normality. Pearson correlation coefficient was used to correlate tumor ADC values on both DWI techniques. Correlation of tumor ADC values with various histopathologic parameters was statistically analyzed by using an independent *t* test. All statistical analysis was done by using statistical software SPSS (version 20.0; SPSS). *P* value <.05 at the CI of 95% was considered significant.

RESULTS

A total of 21 patients (15 males and 6 females) were included in this study, with a median age of 36 months (range 9–72 months) at the time of enucleation. All patients had unilateral tumor (13 right eye and 8 left eye). The median tumor size was 15.3 mm (range 10.2–36 mm). On histopathology, the patients had either poorly differentiated ($n = 13/21$, 61.9%) or moderately differentiated ($n = 8/21$, 38.1%) tumor. Other poor prognostic markers evaluated were optic nerve invasion ($n = 10/21$, 47.6%), choroidal invasion ($n = 12/21$, 57.1%), and anterior eye segment enhancement on postcontrast MR imaging ($n = 6/21$, 28.6%). None of the patients had invasion of the iris, ciliary body, anterior chamber, or sclera on histopathology. The mean duration of clinical follow-up after surgery was 265.4 days (range, 155–410 days). All patients survived during the duration of clinical follow-up, and none developed recurrence. Various demographic and clinical patient characteristics are summarized in Table 2.

Qualitative Image Assessment

HASTE-DWI demonstrated higher image quality scores than EPI-DWI on the overall image quality, artifacts, and tumor sharpness. The average scores for HASTE-DWI versus EPI-DWI were as follows: overall image quality 4.19 versus 3.33, artifacts 4.38 versus 3.67, and tumor sharpness 4.14 versus 3.24 ($P < .001$), respectively. However, the tumor itself was more conspicuous and easily visualized on EPI-DWI compared with HASTE-DWI with an average score of 4.33 versus 3.52 for tumor conspicuity ($P < .001$) (Fig 2). The average acquisition times of EPI-DWI compared with HASTE-DWI were ~1 and 14 minutes, respectively.

Quantitative Image Quality Assessment

In the anteroposterior direction, which is the frequency encoding axis in the scan, the average geometric distortion of orbital diameter on EPI-DWI was 6.105 ± 1.82 mm and on HASTE-DWI was 0.643 ± 0.43 mm ($P < .001$). However, there was no significant difference in distortion of transverse (phase-encoding direction) orbital diameter on EPI-DWI and HASTE-DWI with means of 0.610 ± 0.301 and 0.648 ± 0.339 mm, respectively ($P = .568$). The average SNR of EPI-DWI was 10.616 ± 1.844, 10.268 ± 1.843, and 9.578 ± 1.48 compared with that of 8.283 ± 1.691, 7.875 ± 1.124, and 7.461 ± 1.1 on HASTE-DWI on $b = 0$, 500, and 1000 s/mm^2 ($P < .001$, $P < .001$, and $P < .001$), respectively. The average CNR of EPI-DWI was 10.529 ± 1.553, 10.12 ± 1.254, and 9.4 ± 1.789 compared with that of 8.3 ± 1.527, 7.553 ± 1.33, and 7.295 ± 1.368 on HASTE-DWI on $b = 0$, 500, and 1000 s/mm^2 ($P < .001$, $P < .001$, and $P < .001$), respectively.

The various qualitative and quantitative image quality parameters are summarized in Table 3.

EPI-DWI ADC versus HASTE-DWI ADC Value of the Tumor

The mean tumor ADC value on EPI-DWI was 0.62 ± 0.14 × 10^{-3} mm^2/s (range, 0.41–1.04 × 10^{-3} mm^2/s) and on HASTE-DWI was 0.83 ± 0.17 × 10^{-3} mm^2/s (range, 0.59–1.17 × 10^{-3} mm^2/s). Pearson correlation coefficient was used to correlate tumor ADC values on both DWI techniques. We found a significant correlation of EPI-DWI ADC values with HASTE-DWI ADC values ($r = 0.8$; $P = .01$); however, a linear correlation could not be established. HASTE-DWI ADC values were consistently higher than corresponding EPI-DWI ADC values (Online Supplemental Data).

Correlation of Tumor ADC Values with Prognostic Parameters

The mean and SD of tumor ADC values on both DWI techniques in relation to histopathologic characteristics are shown in Table 4. Lower ADC values were found in tumors with poor

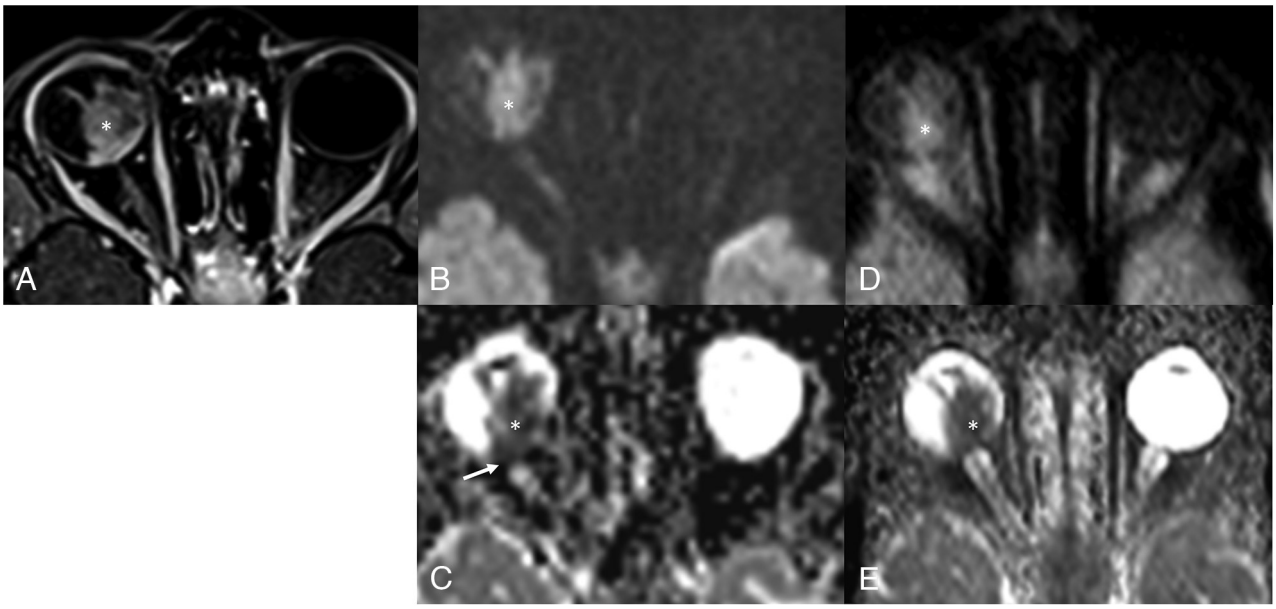

FIG 2. Comparison of EPI-DWI and HASTE-DWI quality. Axial postcontrast T1-weighted image (*A*) shows heterogeneously enhancing mass (*asterisk*) in the posterior segment of the right eye globe. EPI (*B*) and HASTE (*D*) axial DWI (b-value, 1000 s/mm^2) at the same level show high signal intensity in the mass (*asterisk*) with corresponding hypointensity on ADC maps (*C* and *E*, respectively, for EPI-DWI and HASTE-DWI), suggestive of diffusion restriction. There is mild elongation (*arrow* in *C*) of eye globe in EPI ADC map in contrast to maintained shape of globe in HASTE ADC map. However, there is a decreased SNR in case of HASTE-DWI and its ADC map.

Table 3: EPI-DWI versus HASTE-DWI quality assessment

Parameter	EPI-DWI	HASTE-DWI	*P* Value
Qualitative parameters ($n = 21$): 5-point Likert scale			
Overall image quality	3.33	4.19	<.001
Artifacts	3.67	4.38	<.001
Tumor sharpness	3.24	4.14	<.001
Tumor conspicuity	3.52	4.33	<.001
Quantitative parameters ($n = 21$)			
Geometric distortion			
Transverse ocular diameter deviation (mean ± SD)	0.610 ± 0.301 mm	0.648 ± 0.339 mm	.568
Anteroposterior ocular diameter deviation (mean ± SD)	6.105 ± 1.82 mm	0.643 ± 0.43 mm	<.001
SNR			
$b = 0$	10.616 ± 1.844	8.283 ± 1.691	<.001
$b = 500$	10.268 ± 1.843	7.875 ± 1.124	<.001
$b = 1000$	9.578 ± 1.48	7.461 ± 1.1	<.001
CNR			
$b = 0$	10.529 ± 1.553	8.3 ± 1.527	<.001
$b = 500$	10.12 ± 1.254	7.553 ± 1.33	<.001
$b = 1000$	9.4 ± 1.789	7.295 ± 1.368	<.001

prognostic markers, such as poorly differentiated tumor (Fig 3; Online Supplemental Data), postlaminar optic nerve invasion (Fig 4; Online Supplemental Data), presence of choroid invasion (Fig 5; Online Supplemental Data), and large tumor size. The mean tumor ADC values in the presence of these markers ranged from 0.52 to 0.59 $\times$ 10^{-3} mm^2/s on EPI-DWI and 0.69 to 0.81 $\times$ 10^{-3} mm^2/s on HASTE-DWI compared with 0.65 to 0.68 $\times$ 10^{-3} mm^2/s and 0.81 to 0.89 $\times$ 10^{-3} mm^2/s in their absence, respectively; however, none reached a statistically significant difference. A higher mean tumor ADC value 0.7 $\times$ 10^{-3} mm^2/s on EPI-DWI and 0.91 $\times$ 10^{-3} mm^2/s on HASTE-DWI was seen in the presence of anterior eye segment enhancement (Online Supplemental Data) compared with that in its absence (0.58 $\times$ 10^{-3} mm^2/s and 0.8 $\times$ 10^{-3} mm^2/s, respectively); however, the difference was not statistically significant.

DISCUSSION

MR imaging plays a crucial role in diagnosis, staging, and therapeutic planning of patients with RB in the current practice.[16,17] Presence of restricted diffusion on DWI can help in ocular tumor characterization, especially in cases of indeterminate solid masses.[5] Most of the published literature regarding utility of DWI in patients with RB is based on EPI-DWI technique with studies showing encouraging results for potential utility of ADC values as a noninvasive imaging prognostic biomarker.[6-8] However, EPI-based technique has anatomic distortion and

Table 4: Correlation of tumor ADC values on EPI-DWI and HASTE-DWI with prognostic parameters[b]

Prognostic Parameter	Mean ADC Value for EPI-DWI ($\times 10^{-3}$ mm^2/s)	*P* Value for EPI-DWI	Mean ADC Value for HASTE-DWI ($\times 10^{-3}$ mm^2/s)	*P* Value for HASTE-DWI
Tumor grade				
Poorly differentiated ($n = 13$)	0.59 ± 0.16	.37	0.79 ± 0.16	.22
Moderately differentiated ($n = 8$)	0.65 ± 0.09		0.89 ± 0.18	
Tumor size				
<15 mm ($n = 9$)	0.66 ± 0.16	.2	0.89 ± 0.19	.14
>15 mm ($n = 12$)	0.58 ± 0.11		0.78 ± 0.14	
Optic nerve invasion				
Absent ($n = 11$)	0.65 ± 0.17	.35[b]	0.88 ± 0.20	.14[b]
Prelaminar ($n = 5$)	0.64 ± 0.07		0.86 ± 0.13	
Postlaminar ($n = 5$)	0.52 ± 0.04		0.69 ± 0.05	
Choroid invasion				
Present ($n = 12$)	0.57 ± 0.11	.086	0.81 ± 0.18	.66
Absent ($n = 9$)	0.68 ± 0.15		0.85 ± 0.16	
Anterior eye segment enhancement on postcontrast MRI				
Present ($n = 6$)	0.70 ± 0.18	.056	0.91 ± 0.23	.15
Absent ($n = 15$)	0.58 ± 0.10		0.80 ± 0.13	

[a]Other histopathologic characteristics (eg, invasion of iris, ciliary body, anterior chamber, and sclera) were not found in any patient.
[b]*P* value is for ADC values in cases with postlaminar invasion versus cases with prelaminar or absent invasion.

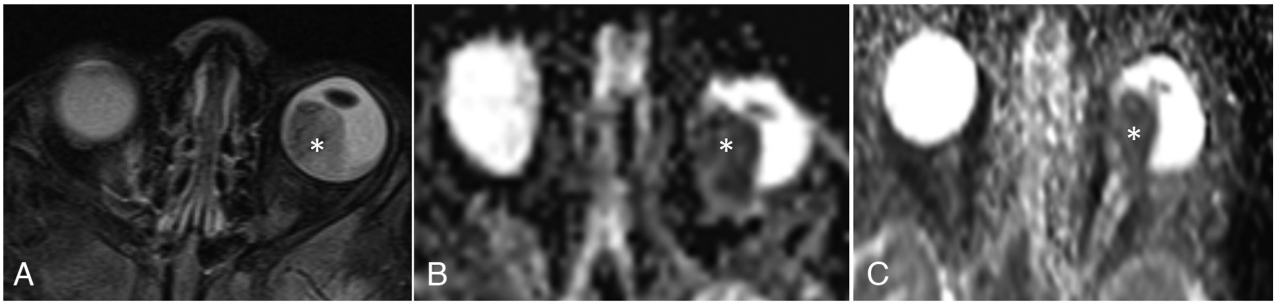

FIG 3. Poorly differentiated RB on histopathology. Axial T2-weighted image (*A*) shows a heterogeneously hypointense mass (*asterisk*) occupying the posterior segment of left eye globe. EPI (*B*) and HASTE (*C*) ADC maps show corresponding hypointense signal in the mass, suggestive of diffusion restriction. Mass showed low ADC values on both EPI-DWI and HASTE-DWI (mean ADC value being 0.48 $\times 10^{-3}$ mm^2/s and 0.70 $\times 10^{-3}$ mm^2/s for EPI-DWI and HASTE-DWI, respectively).

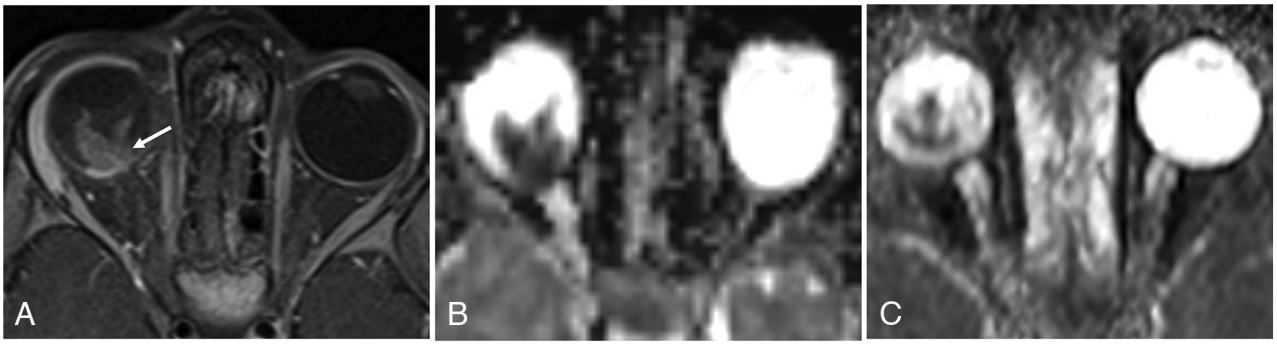

FIG 4. Histopathologically proved optic nerve invasion. Axial postcontrast T1-weighted image (*A*) at same level shows homogeneously enhancing mass with abnormal thickening and enhancement in the optic disc extending in postlaminar part of optic nerve (*arrow*), suggestive of postlaminar optic nerve invasion. EPI (*B*) and HASTE (*C*) ADC maps at the same level show corresponding hypointensity suggestive of diffusion restriction. Mass showed low ADC values on both EPI-DWI and HASTE-DWI (mean ADC value being 0.52 $\times 10^{-3}$ mm^2/s and 0.67 $\times 10^{-3}$ mm^2/s for EPI-DWI and HASTE-DWI, respectively).

magnetic susceptibility-induced artifacts in orbital imaging. In this study, we showed that, although HASTE-DWI, which is one of the non–EPI-based DWI techniques, had superior image quality and less geometric distortion than EPI-DWI, it lagged in terms of tumor conspicuity, SNR, and CNR; it showed no significant benefit in tumor characterization by using ADC maps. Both techniques produced diagnostic quality DWI enabling tumor delineation. Also, because all of the tumors in our study were either medium or large-sized (>10 mm in size), susceptibility artifacts in EPI-DWI did not appreciably affect tumor evaluation in any case.

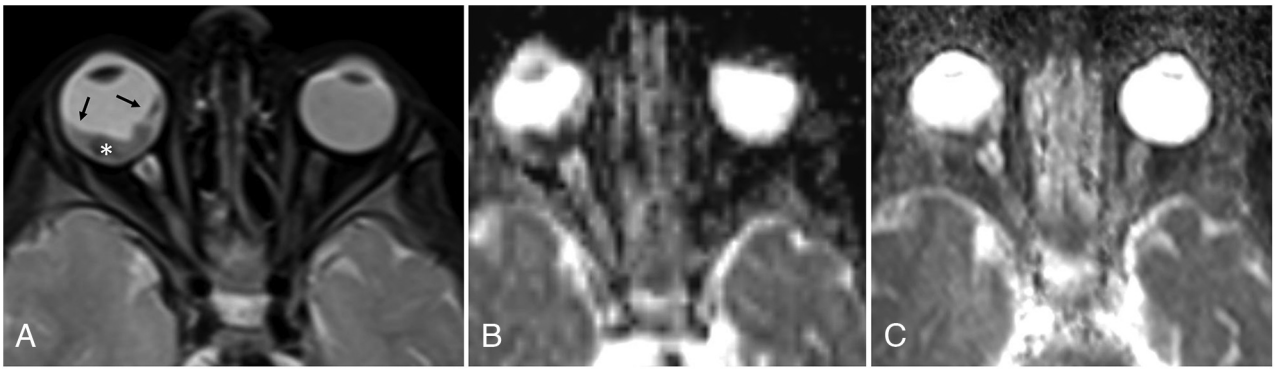

FIG 5. Histopathologically proved choroid invasion. Axial T2-weighted image (*A*) shows a hypointense small mass in the posterior segment of right eye with associated retinal detachment (*arrows*). EPI (*B*) and HASTE (*C*) ADC maps show corresponding hypointensity on ADC maps suggestive of diffusion restriction. Mass showed low ADC values on both EPI and HASTE-DWI (mean ADC value being 0.51 $\times$ 10^{-3} mm^2/s and 0.87 $\times$ 10^{-3} mm^2/s for EPI-DWI and HASTE-DWI, respectively).

This is especially relevant in our cohort where RB is usually diagnosed at a later stage with larger tumor size due to lack of a routine RB screening program at birth or in neonates and infants.[18-20]

Markedly longer acquisition times of the order of >10 times in HASTE-DWI MR imaging compared with EPI-DWI was a major drawback, especially as it prolongs the duration of general anesthesia, potentially risking the attendant complications in these children. Longer acquisition time of HASTE-DWI MR imaging is a consequence of its inherently low SNR, which must be compensated for by obtaining multiple signal averages.

We further correlated tumor ADC values obtained on both EPI-DWI and HASTE-DWI with histopathologic prognostic parameters. We found lower ADC values (0.52–0.59 $\times$ 10^{-3} mm^2/s on EPI-DWI and 0.69–0.81 $\times$ 10^{-3} mm^2/s on HASTE-DWI) in tumors with adverse prognostic histopathologic factors; however, the difference was not statistically significant. These results are in keeping with the overall ambivalent results of the previous studies showing ADC correlation with some of the prognostic parameters and absence of any association with others (Online Supplemental Data). The lack of statistically significant ADC values in our study could be ascribed to a multitude of factors: use of 1.5T MR imaging, standard head coil rather than orbital surface coil, small sample size, relatively larger mean tumor size, and only few well or moderately differentiated tumors. Another factor limiting the clinical correlation of ADC values as an imaging biomarker for poor prognostic features of RB is its high variability (0.38 $\times$ 10^{-3} to 0.74 $\times$ 10^{-3} mm^2/s) and lack of definite cutoff values.[6-8] In our study, we found that mean tumor ADC values were consistently higher in HASTE-DWI compared with EPI-DWI. While there was significant correlation between the ADC values obtained from both techniques, no linear correlation was found. This variability in the numerical values further complicates the use of ADC values in RB as a tool for the interpreting radiologist.

Previous studies have demonstrated a correlation of anterior segment enhancement on postcontrast MR imaging with aggressive tumor behavior including invasion of the optic nerve and choroid.[21-23] To our knowledge, no study has correlated tumor ADC value with anterior segment enhancement. In our study, we found that eyes showing anterior segment enhancement had higher tumor ADC values (0.7 $\times$ 10^{-3} mm^2/s on EPI-DWI and 0.91 $\times$ $10^{-3}/mm^2/s$ on HASTE-DWI), contrary to the expected low ADC values associated with aggressive tumors. However, this difference was not found to be statistically significant. Enhancement of the anterior eye segment on postcontrast MR imaging in RB is recognized to be either due to hyperemia secondary to iris neovascularization (rubeosis iridis) or secondary to infiltration by the tumor itself. Of note, no tumor showed anterior segment invasion on histopathology in our study. Thus, anterior eye segment enhancement in our cases is presumably due to tumor-induced aseptic cellulitis and consequent hyperemia. Higher ADC values in these tumors may be a result of areas of necrosis that were inadvertently included in the ROIs.

Apart from having a relatively small sample size, our study had a few other limitations. The measured mean ADC value from the entire tumor may not be truly representative of the whole tumor presumably due to tumor heterogeneity. More than one prognostic factor was present in several patients. Therefore, the low ADC values cannot be ascribed to any one particular poor prognostic parameter (confounding factors). Inadvertent inclusion of some part of necrotic tumor in the ROI placed for tumor ADC calculation may have led to falsely high ADC values. Correlation of data with long-term survival or mortality outcomes could not be done.

CONCLUSIONS

Although HASTE-DWI is a frequently used sequence in MR imaging protocols for detection of cholesteatomas, most of the centers do not use this sequence for orbital MR imaging. Our study further reiterates the limitations and lack of any incremental benefit of including non-EPI-DWI in an orbital MR imaging protocol for children with RB. In conclusion, although HASTE-DWI shows an improved overall image quality with less orbital distortion and artifacts, it lacks in terms of tumor conspicuity, SNR, and CNR compared with EPI-DWI. ADC values derived from HASTE-DWI show no advantage over EPI-DWI in correlation with histopathologic prognostic markers in RB. A major drawback of HASTE-DWI is its markedly long acquisition time prolonging the duration of general anesthesia for MR imaging.

Disclosure forms provided by the authors are available with the full text and PDF of this article at www.ajnr.org.

REFERENCES

1. Koh DM, Collins DJ. **Diffusion-weighted MRI in the body: applications and challenges in oncology.** *AJR Am J Roentgenol* 2007;188:1622–35 CrossRef Medline
2. Cameron CA, Tong JY, Juniat V, et al. **Diagnostic utility of diffusion-weighted imaging and apparent diffusion coefficient for common orbital lesions: a review.** *Ophthalmic Plast Reconstr Surg* 2022;38:515–21 CrossRef Medline
3. Politi LS, Forghani R, Godi C, et al. **Ocular adnexal lymphoma: diffusion-weighted MR imaging for differential diagnosis and therapeutic monitoring.** *Radiology* 2010;256:565–74 CrossRef Medline
4. Sepahdari AR, Aakalu VK, Kapur R, et al. **MRI of orbital cellulitis and orbital abscess: the role of diffusion-weighted imaging.** *AJR Am J Roentgenol* 2009;193:W244–50 CrossRef Medline
5. Sepahdari AR, Aakalu VK, Setabutr P, et al. **Indeterminate orbital masses: restricted diffusion at MR imaging with echo-planar diffusion-weighted imaging predicts malignancy.** *Radiology* 2010;256:554–64 CrossRef Medline
6. Abdel Razek AA, ElKhamary S, Al-Mesfer S, et al. **Correlation of apparent diffusion coefficient at 3T with prognostic parameters of retinoblastoma.** *AJNR Am J Neuroradiol* 2012;33:944–48 CrossRef Medline
7. Cui Y, Luo R, Wang R, et al. **Correlation between conventional MR imaging combined with diffusion-weighted imaging and histopathologic findings in eyes primarily enucleated for advanced retinoblastoma: a retrospective study.** *Eur Radiol* 2018;28:620–29 CrossRef Medline
8. Sepahdari AR, Kapur R, Aakalu VK, et al. **Diffusion-weighted imaging of malignant ocular masses: initial results and directions for further study.** *AJNR Am J Neuroradiol* 2012;33:314–19 CrossRef Medline
9. Le Bihan D, Poupon C, Amadon A, et al. **Artifacts and pitfalls in diffusion MRI.** *J Magn Reson Imaging* 2006;24:478–88 CrossRef Medline
10. Benson JC, Carlson ML, Lane JI. **Non-EPI versus multishot EPI DWI in cholesteatoma detection: correlation with operative findings.** *AJNR Am J Neuroradiol* 2021;42:573–77 CrossRef Medline
11. Dudau C, Draper A, Gkagkanasiou M, et al. **Cholesteatoma: multishot echo-planar vs non echo-planar diffusion-weighted MRI for the prediction of middle ear and mastoid cholesteatoma.** *BJR Open* 2019;1:20180015 CrossRef Medline
12. Schwartz KM, Lane JI, Bolster BD Jr, et al. **The utility of diffusion-weighted imaging for cholesteatoma evaluation.** *AJNR Am J Neuroradiol* 2011;32:430–36 CrossRef Medline
13. Amoodi H, Mofti A, Fatani NH, et al. **Non-echo planar diffusion-weighted imaging in the detection of recurrent or residual cholesteatoma: a systematic review and meta-analysis of diagnostic studies.** *Cureus* 2022;14:e32127 CrossRef Medline
14. de Graaf P, Pouwels PJ, Rodjan F, et al. **Single-shot turbo spin-echo diffusion-weighted imaging for retinoblastoma: initial experience.** *AJNR Am J Neuroradiol* 2012;33:110–18 CrossRef Medline
15. Hiwatashi A, Togao O, Yamashita K, et al. **3D turbo field echo with diffusion-sensitized driven-equilibrium preparation technique (DSDE-TFE) versus echo planar imaging in evaluation of diffusivity of retinoblastoma.** *Br J Radiol* 2016;89:20160074 CrossRef Medline
16. Silvera VM, Guerin JB, Brinjikji W, et al. **Retinoblastoma: what the neuroradiologist needs to know.** *AJNR Am J Neuroradiol* 2021;42:618–26 CrossRef Medline
17. de Graaf P, Göricke S, Rodjan F, European Retinoblastoma Imaging Collaboration (ERIC), et al. **Guidelines for imaging retinoblastoma: imaging principles and MRI standardization**. *Pediatr Radiol* 2012;42:2–14 CrossRef Medline
18. Singh U, Katoch D, Kaur S, et al. **Retinoblastoma: a sixteen-year review of the presentation, treatment, and outcome from a tertiary care institute in Northern India.** *Ocul Oncol Pathol* 2017;4:23–32 CrossRef Medline
19. Yan J, Zhang H, Li Y. **Establishment of the relationship between tumor size and range of histological involvement to evaluate the rationality of current retinoblastoma management.** *PLoS One* 2013;8:e80484 CrossRef Medline
20. Vempuluru VS, Kaliki S. **Screening for retinoblastoma: a systematic review of current strategies.** *Asia Pac J Ophthalmol (Phila)* 2021;10:192–99 CrossRef Medline
21. de Graaf P, van der Valk P, Moll AC, et al. **Contrast-enhancement of the anterior eye segment in patients with retinoblastoma: correlation between clinical, MR imaging, and histopathologic findings.** *AJNR Am J Neuroradiol* 2010;31:237–45 CrossRef Medline
22. Galluzzi P, Cerase A, Hadjistilianou T, et al. **Retinoblastoma: abnormal gadolinium enhancement of anterior segment of eyes at MR imaging with clinical and histopathologic correlation.** *Radiology* 2003;228:683–90 CrossRef Medline
23. Deike-Hofmann K, von Lampe P, Eerikaeinen M, et al. **Anterior chamber enhancement predicts optic nerve infiltration in retinoblastoma.** *Eur Radiology* 2022;32:7354–64 CrossRef Medline